Electron-energy-loss spectroscopy of multilayered materials: Theoretical aspects and study of interface optical phonons in semiconductor superlattices

Ph. Lambin, J. P. Vigneron, and A. A. Lucas
Département de Physique, Facultés Universitaires Notre Dame de la Paix, 61 rue de Bruxelles, B-5000 Namur, Belgium
(Received 4 June 1985)

The dielectric theory of electron-energy-loss spectroscopy (EELS) in the reflection geometry is reformulated so as to allow for an arbitrary compositional variation of the target material in the direction perpendicular to its surface. A new, general expression for the energy-loss spectrum is obtained in terms of an exact "effective dielectric function." It is shown that the effective dielectric function, valid at long wavelength, can be obtained by solving a Riccati differential equation, the only information required being the otherwise arbitrary profile, in the normal direction z, of the dielectric constant $\epsilon(\omega,z)$ for the frequency region of interest. Attention is then paid to an idealized multilayered material, made of an arbitrary succession of homogeneous layers separated by sharp interfaces parallel to the free surface. If $\epsilon(\omega,z)$ is assumed to take constant values within each layer, an original solution is obtained for the Riccati equation, giving the effective dielectric function of the material in the form of a continued fraction. For the thick periodic multilayers or superlattices of current interest, the continued fraction can be evaluated analytically. Applications will be presented for the phonon EELS spectrum of polar-semiconductor superlattices for which a Lorentzian model for the ω dependence of the infrared dielectric constant can be used. Two kinds of vibrational excitations are theoretically predicted in such superlattices: (i) Bloch-like, Fuchs-Kliewer interface modes, propagating throughout the layers; and (ii) evanescent, Fuchs-Kliewer surface or interface modes. It is shown that the Bloch modes are responsible for weak EELS continua, while the localized modes give rise to strong peaks in the spectrum. Furthermore, it is predicted that the main features of the EELS spectrum sensitively depend on the relative thicknesses of the two alternating layers of the superlattice.

I. INTRODUCTION

During the past 15 years, electron-energy-loss spectroscopy (EELS) in the reflection geometry has emerged as a reliable technique for studying clean or contaminated surfaces. In this technique, monochromatized electrons backscattered from the surface of a target material are analyzed in energy to detect losses and gains characteristic of surface plasma or vibrational excitations. First restricted to conducting targets, high resolution EELS experiments have recently been successfully performed with insulators and poorly conducting materials,[1] so that this technique is now generally applicable as a powerful spectroscopic tool for the study of any material surface.

In the meantime, the theoretical framework for interpreting the EELS spectra has been developed.[2,3] An adequate theoretical approach to EELS is provided by the so-called dielectric theory,[2,4] where the electrons are considered as classical particles, while the multiple absorption or emission of phonons or plasmons are quantum mechanically described. In addition to its intrinsic simplicity, this "semiquantum" theory has been shown to be in remarkable agreement with the recent experimental spectra obtained on selected isotropic or anisotropic thick insulators.[5,6]

In the infrared range, the EELS spectrum of a poorly conducting, partly ionic crystal shows narrow multiple-loss (and -gain) peaks due to emission (and absorption) of macroscopic, Fuchs-Kliewer surface phonons, and the strengths of the multiple-loss peaks follow a Poisson distribution. These phonons at a thick isotropic insulator surface have frequencies ω such that $\epsilon(\omega)=-1$, where $\epsilon(\omega)$ denotes the bulk dielectric constant of the material. In the dielectric theory of EELS, these frequencies generate δ-like peaks in the so-called surface loss function[7] $\mathrm{Im}\{-1/[\epsilon(\omega)+1]\}$.

It turns out that the dielectric theory can still be applied to anisotropic crystals, provided $\epsilon(\omega)$ in the loss function be replaced by an appropriate effective dielectric function $\xi(\mathbf{k},\omega)$, where $\mathbf{k}$ denotes the wave vector of the surface phonons.[6] It is remarkable that the same result holds equally true when the dielectric constant (or tensor) of the target material is an arbitrary function of the coordinate z below the surface.[8] In this paper, we indeed prove that the relevant effective dielectric function is equal to the surface value of the ratio of the displacement vector perpendicular to the surface, and the projection of the electric polarization field onto the direction of the surface wave vector $\mathbf{k}$. Furthermore, it is shown here for the first time that $\xi(\mathbf{k},\omega)$ can be obtained by solving a Riccati differential equation, where $\epsilon(\omega,z)$ enters as the only input. For illustrative purpose, emphasis will be put here on a target material made of an arbitrary succession of parallel layers, with the (nonessential) simplifying assumption that $\epsilon(\omega,z)$ takes constant values $\epsilon_i(\omega)$ within the successive layers $i=1,2,3,\ldots$. Such a histogramlike model for

$\epsilon(\omega,z)$ leads to a continued-fraction expansion of the effective dielectric function of the material.

The continued-fraction solution of the Riccati equation is a new, powerful result as it provides us with a simple formulation of the effective susceptibility of any stratified material or multilayered heterostructure. Moreover, it is very convenient for algebraic analyses and also for numerical computations. Besides, the continued-fraction formulation can easily be generalized to include retardation effects,[9] although these effects are irrelevant to the present EELS context. For illustration, attention will be paid here to synthesized semiconductor superlattices, which have attracted a growing interest during the past several years.[10] Detailed applications will be considered for semi-infinite superlattices as well as for superlattices with a finite number of periods.

Our analysis is complementary of a recent theoretical work devoted to collective plasmon excitations in superlattices.[11] The authors of this latter work have computed the EELS spectrum of a semi-infinite superlattice formed from metallic layers intercalated with slabs made of a nondispersive medium. By solving Poisson's equation in the layers, and by applying the usual boundary conditions at the interfaces, Camley and Mills[11] were able to deduce the nonretarded electromagnetic eigenmodes of the superlattice. Besides continuum eigenmodes which are a consequence of Bloch's theorem, Camley and Mills found localized branches of surface and interface modes. By contrast with the Bloch solutions of Poisson's equation,[12] the localized modes correspond to evanescent solutions which are a consequence of the loss of periodicity near the terminating layer of the superlattice,[11,13] and these new modes influence the EELS spectrum of the structure.

In the new formalism of the effective dielectric function that is presented in this paper, the localized, Fuchs-Kliewer modes correspond to wave vectors $\mathbf{k}$ such that $\xi(\mathbf{k},\omega)=-1$, while the continua are related to complex values of ξ. Although the validity of the general formalism we have developed does not rest upon any particular ω dependence for the dielectric constants $\epsilon_i(\omega)$, we will deal particularly with the infrared optical vibrational properties of superlattices made of cubic binary compounds. The vibrational Fuchs-Kliewer modes of the superlattice will be described from the expression obtained for the loss function $\mathrm{Im}\{-1/[\xi(\mathbf{k},\omega)+1]\}$, which embodies the general linear response of the EELS probe. We will study the EELS spectrum of selected semiconductor superlattices and will show that the continuously distributed Fuchs-Kliewer states give rise to weak features in the EELS spectrum, while the localized vibrational modes are responsible for strong peaks in the spectrum. As an important result, it will be shown that the detailed shape of the spectrum depends rather sensitively on the ratio of the layer thicknesses in the superlattice. This feature amounts to a proof of the capability of the EELS technique to probe the dielectric properties of the material several hundred angstroms deep under the surface.

II. THEORY OF EELS SPECTRUM

Electron-energy-loss spectra obtained in the reflection geometry at the surface of a semi-infinite medium can be theoretically treated within the framework of the so-called dielectric theory.[4] In this theory, the electron is considered as a classical particle, while the collective excitations of the medium (such as optical phonons or plasmons) are described quantum mechanically. The dielectric theory proceeds in two steps. The first step consists in evaluating the work done by the polarization field of the sample on the electron (responsible for the polarization) along its classical trajectory.[2,3] In this classical step, the work

$$W=-e\int_{-\infty}^{+\infty}\mathbf{v}_e(t)\cdot\mathbf{E}(\mathbf{r}_e(t),t)dt \tag{2.1}$$

is written as the first moment of a classical energy-loss probability $P_{\mathrm{cl}}(\omega)$:

$$W=\int_0^{\infty}\hbar\omega P_{\mathrm{cl}}(\omega)d\omega\ , \tag{2.2}$$

where $\hbar\omega$ denotes the energy loss. In Eq. (2.1), $\mathbf{r}_e(t)$ is the trajectory of the electron (charge e), $\mathbf{v}_e(t)$ is the electron velocity, and $\mathbf{E}(\mathbf{r},t)$ denotes the polarization field of the material under consideration.

This first, classical step is complemented by a suitable quantum-mechanical description of the multiple excitations emitted or absorbed by the electron. The essential result of the second step of the EELS theory is the following expression of the full energy-loss probability for a target material at temperature T:[2,5]

$$P(\omega,T)=\frac{1}{2\pi}P_0(T)\int_{-\infty}^{+\infty}\exp[P_{\mathrm{cl}}(t,T)]e^{i\omega t}dt\ , \tag{2.3}$$

where

$$P_{\mathrm{cl}}(t,T)=\tfrac{1}{2}\int_0^{\infty}P_{\mathrm{cl}}(\omega')\left[e^{-i\omega' t}\left[\coth\frac{\hbar\omega'}{2k_BT}+1\right]+e^{+i\omega' t}\left[\coth\frac{\hbar\omega'}{2k_BT}-1\right]\right]d\omega'\ . \tag{2.4}$$

In Eq. (2.4) the prefactor $P_0(T)$, given by

$$P_0(T)=\exp\left[-\int_0^{\infty}P_{\mathrm{cl}}(\omega')\coth\left[\frac{\hbar\omega'}{2k_BT}\right]d\omega'\right]\ , \tag{2.5}$$

ensures the normalization of the loss spectrum at all temperatures.

From a numerical point of view, it is worth noticing that the transformations from the classical energy-loss probability $P_{\mathrm{cl}}(\omega)$ to the full EELS spectrum $P(\omega,T)$ proceeds by way of two Fourier transforms which can be efficiently carried out (fast Fourier-transform technique). Also, the theoretical EELS spectrum of Eq. (2.3) can be further broadened to include instrumental resolution by convoluting $P(\omega,T)$ with the spectrometer response function, the width of which being adjusted so as to reproduce the experimental width of the elastic peak [which is represented as a Dirac δ function located at $\omega=0$ in the theoretical spectrum of Eq. (2.3)]. Finally, we note that the full EELS spectrum given by Eqs. (2.3) and (2.4) has multiple-loss peaks which follow a Poisson distribution.

We now turn our attention to the classical work. For

fast electrons it is sufficient, in general, to consider the unperturbed classical trajectory, as if the dynamics of the electron were unaffected by the force of the polarization field which acts on it. Furthermore, neglecting the image force as well,[4] $\mathbf{r}_e(t)$ is assumed to obey the following simple law:

$$\mathbf{r}_e(t)=t\mathbf{v}_{||}+|tv_\perp|\mathbf{n}\ , \tag{2.6}$$

where $\mathbf{v}_{||}$ is the electron velocity component parallel to the surface of the material, $v_\perp$ is the normal component of the velocity, and $\mathbf{n}$ denotes the unit outward normal at the surface (Fig. 1). Throughout this paper the coordinate z is oriented parallel to the outward normal $\mathbf{n}$, the surface coinciding with the plane $z=0$ and negative z corresponding to the material region. When writing Eq. (2.6), it has been assumed that the specular reflection of the electron occurs at time $t=0$ at the origin of the coordinates, the effects of the collision change the sign of the electron velocity along the normal direction $\mathbf{n}$. In addition, the penetration of the electron below the assumed abrupt surface is not taken into account, this simplifying assumption being fully justified for phonon excitations by a low energy electron (a few eV).[4]

Retardation effects in the electric field being ignored (retardation effects are actually negligible in present resolution EELS), the polarization field $\mathbf{E}(\mathbf{r},t)$ is Fourier transformed with respect to the coordinates x and y parallel to the surface and with respect to the time t:

$$\mathbf{E}(\mathbf{r},t)=\int d^2k\int_{-\infty}^{+\infty}d\omega\,\mathbf{E}(\mathbf{k},\omega,z)e^{i(k_xx+k_yy-\omega t)}\ , \tag{2.7}$$

where $\mathbf{k}=(k_x,k_y)$ is a two-dimensional wave vector. Taking into account Eq. (2.6) and the nonretarded limit $[\nabla\times\mathbf{E}(\mathbf{r},t)=0]$, it is straightforward to calculate the expression of the classical work W [Eq. (2.1)], and then the following expression of $P_{\rm cl}(\omega)$:

$$P_{\rm cl}(\omega)=\int d^2k\frac{-4e}{\hbar\Omega}\int_0^\infty\sin(\Omega z/v_\perp)\mathrm{Im}E_\perp(\mathbf{k},\omega,z)dz\ , \tag{2.8}$$

where $\Omega=\omega-\mathbf{k}\cdot\mathbf{v}_{||}$. Integration by part, complemented by the condition $\nabla\cdot\mathbf{E}(\mathbf{r},t)=0$ $(z>0)$ finally yields the following result:

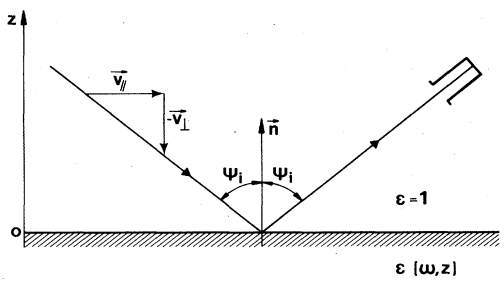

FIG. 1. Definition of the geometrical parameters relevant to the theory of EELS in the reflection geometry. Throughout this paper the coordinate z is measured in the direction perpendicular to the free surface of the sample, which extends from $z=0$ (surface) to $z=-\infty$.

$$P_{\rm cl}(\omega)=\mathrm{Im}\left[\frac{-4e}{\hbar}v_\perp\int\frac{E_\perp(\mathbf{k},\omega,+0)}{\Omega^2+(kv_\perp)^2}d^2k\right]\ . \tag{2.9}$$

This expression relates the classical loss spectrum to the Fourier transform of the normal component of the polarization field at the surface $z=0$, computed from above the surface.

The electric field above the surface (region $z>0$) is the sum of the polarization field $\mathbf{E}(\mathbf{r},t)$ and the (nonretarded) Coulomb field $\mathbf{E}_e(\mathbf{r},t)$ of the electron, given by

$$\mathbf{E}_e(\mathbf{r},t)=-\nabla V_e(\mathbf{r},t)=-\nabla\frac{e}{|\mathbf{r}-\mathbf{r}_e(t)|}\ . \tag{2.10}$$

Below the surface, the electric field $\mathbf{E}(\mathbf{r},t)$ satisfies $\nabla\times\mathbf{E}=0$ and $\nabla\cdot\epsilon\mathbf{E}=0$. In terms of the Fourier transform of $\mathbf{E}(\mathbf{r},t)$ [Eq. (2.7)], we now introduce the following quantity:[14]

$$\xi(\mathbf{k},\omega,z)=i\frac{\mathbf{D}(\mathbf{k},\omega,z)\cdot\mathbf{n}}{\mathbf{E}(\mathbf{k},\omega,z)\cdot\mathbf{k}/k}\ , \tag{2.11}$$

with $\mathbf{D}(\mathbf{k},\omega,z)=\epsilon(\omega,z)\mathbf{E}(\mathbf{k},\omega,z)$, where $\epsilon(\omega,z)$ is the long-wavelength dielectric constant (tensor) of the material, which may be a function of the coordinate z. Even in the presence of sharp interfaces parallel to the x,y directions below the surface (such as in the multilayered materials considered below), $\xi(\mathbf{k},\omega,z)$ is a continuous function of z, owing to the usual boundary conditions at such interfaces (continuity of the normal component of $\mathbf{D}$ and of the parallel component of $\mathbf{E}$). The specific properties of the quantity $\xi(\mathbf{k},\omega,z)$ are analyzed in the next section, but it is worth mentioning here that for a semi-infinite isotropic medium $\xi(\mathbf{k},\omega,z)$ reduces to the dielectric constant $\epsilon(\omega)$ of the medium.

It now becomes straightforward to establish the following expressions, taking account of the definition of $\xi(\mathbf{k},\omega,z)$ and the boundary conditions at the surface:

$$\begin{aligned}E_\perp(\mathbf{k},\omega,+0)&=D_\perp(\mathbf{k},\omega,-0)-E_{e\perp}(\mathbf{k},\omega,0)\\&=-i\xi_0\mathbf{k}\cdot\mathbf{E}_{||}(\mathbf{k},\omega,-0)/k-E_{e\perp}(\mathbf{k},\omega,0)\\&=-i\xi_0\mathbf{k}\cdot[\mathbf{E}_{||}(\mathbf{k},\omega,+0)+\mathbf{E}_{e||}(\mathbf{k},\omega,0)]/k\\&\quad-E_{e\perp}(\mathbf{k},\omega,0)\ ,\end{aligned} \tag{2.12}$$

where ξ_0 is a short writing for $\xi(\mathbf{k},\omega,-0)$ computed at the surface. As in vacuum $(z>0$ region)

$$i\,\mathbf{k}\cdot\mathbf{E}_{||}(\mathbf{k},\omega,z)/k=E_\perp(\mathbf{k},\omega,z)\ ,$$

the above relation can be rewritten as

$$\begin{aligned}(1+\xi_0)E_\perp(\mathbf{k},\omega,+0)&=-i\xi_0\mathbf{k}\cdot\mathbf{E}_{e||}(\mathbf{k},\omega,0)/k-E_{e\perp}(\mathbf{k},\omega,0)\\&=-k\xi_0V_e(\mathbf{k},\omega,0)\\&\quad+\left[\frac{\partial}{\partial z}V_e(\mathbf{k},\omega,z)\right]_{z=0}\ ,\end{aligned} \tag{2.13}$$

where $V_e(\mathbf{k},\omega,z)$ denotes the Fourier transform of the Coulomb potential of the electron [refer to Eq. (2.10)]. The above formulation shows that, in the absence of

external excitation ($V_e=0$), the polarization field $\mathbf{E}(\mathbf{k},\omega,z)$ in vacuum ($z>0$) vanishes, unless

$$\xi_0=\xi(\mathbf{k},\omega,0)=-1 . \tag{2.14}$$

The regions of $\mathbf{k}$ and ω, where that condition is fulfilled, correspond to the nonretarded electromagnetic eigenmodes of the material. Equation (2.14) is a generalization of the well-known condition $\epsilon(\omega)=-1$ giving the nonretarded eigenmodes of a semi-infinite isotropic medium with dielectric constant $\epsilon(\omega)$.[15] For that reason, ξ_0 can be regarded as the effective dielectric function of the material.

We now return to expression (2.9) of the classical loss probability. Having computed the Fourier transform $V_e(\mathbf{k},\omega,z)$ of the electron Coulomb potential, using the simple law (2.6) for the electron trajectory, and replacing $E_\perp(\mathbf{k},\omega,+0)$ by its expression deduced from Eq. (2.13), we end up with the following result:

$$P_{\rm cl}(\omega)=\frac{4}{\pi^2}\frac{e^2}{\hbar v_\perp}\int_D d^2k\frac{1}{k^2}\frac{(kv_\perp)^3}{[(\omega-\mathbf{k}\cdot\mathbf{v}_{||})^2+(kv_\perp)^2]^2}\times\mathrm{Im}\frac{-1}{\xi_0(\mathbf{k},\omega)+1} . \tag{2.15}$$

In Eq. (2.15), the integration is performed over a domain D including all surface wave vectors $\mathbf{k}$ which, through energy and momentum conservations, scatter the reflected electron towards the detector aperture. In polar coordinates, the polar angle ϕ of $\mathbf{k}$ being measured with respect to $\mathbf{v}_{||}$, D is the domain bounded by a closed curve $k_c(\phi)$ which can be approximated by the ellipse of equation

$$\frac{1}{k_c^2}=\frac{\sin^2(\phi)}{k_{\max}^2}+\frac{\cos^2(\phi)}{[k_{\max}\cos(\psi_i)]^2} , \tag{2.16}$$

where ψ_i is the incidence angle of the electron with respect to the surface normal $\mathbf{n}$ and $k_{\max}=k_e\psi_a$, ψ_a being half the angular aperture of the detector and k_e denotes the de Broglie wave vector of the incident electron. Typically, $k_{\max}=0.04$ Å^{-1}.

III. PROPERTIES OF THE EFFECTIVE DIELECTRIC FUNCTION

The effective dielectric function of the medium has been defined in the preceding section as the value taken at the surface ($z=0$) by the quantity $\xi(\mathbf{k},\omega,z)$ introduced in Eq. (2.11). In this section, some properties of this crucial quantity are presented, with the simplifying assumption that the material is isotropic (anisotropic materials have been considered in previous publications[5,6]). In addition to the simplification of ξ_0 resulting from the assumption of an isotropic target material, the two-dimensional k integration in Eq. (2.15) can further be simplified, as we show in the Appendix. In this section, the frequency ω is considered as a parameter to which the long-wavelength dielectric constant ϵ is related. For a given value of ω, ϵ is assumed to be a function of the coordinate z.

A. Effective dielectric function of an isotropic material

For isotropic media, ξ does not depend on the polar angle of the two-dimensional wave vector $\mathbf{k}$. As a result, Eq. (2.11) can be rewritten as

$$\xi(k,\omega,z)=\left[\frac{\epsilon(\omega,z)}{k}\frac{\partial}{\partial z}V(k,\omega,z)\right]\Big/V(k,\omega,z) , \tag{3.1}$$

where $V(k,\omega,z)$ is the Fourier transform of the polarization potential. For obvious typographical simplifications, we will omit the (k,ω) dependence of ϵ and V and regard these quantities as functions of z. Due to Poisson's equation, the polarization potential in the medium satisfies the second-order differential equation

$$\frac{d}{dz}\left[\epsilon\frac{dV}{dz}\right]-\epsilon k^2V=0 , \tag{3.2}$$

where ϵ is allowed to be a function of z. The boundary condition associated with Eq. (3.2) is $V(z)$ finite as z approaches $-\infty$. Let $V_1(z)$ and $V_2(z)$ be two independent solutions of the above equation. If one of these solutions, say V_1, satisfies that condition, while the other diverges at $z=-\infty$, then the divergent solution V_2 must be discarded when writing the solution of Eq. (3.2). In these conditions $\xi(z)$, as deduced from Eq. (3.1), is

$$\xi(z)=\frac{\epsilon(z)}{k}\frac{1}{V_1(z)}\frac{dV_1(z)}{dz} . \tag{3.3}$$

Consequently, $\xi(z)$ [and $\xi_0=\xi(0)$ as well] is uniquely defined in that case; it is given by Eq. (3.3) where $V_1(z)$ is the regular solution of Poisson's equation. For instance, suppose that $\epsilon(z)$ takes an asymptotic constant value ϵ_s far away from the surface (ϵ_s could be the dielectric constant of the substrate on which a film has been deposited). Hence, the Poisson equation possesses a set of independent solutions behaving as $V_1(z)\sim\exp(kz)$ and $V_2(z)\sim\exp(-kz)$ at $z=-\infty$. Elimination of the dominant solution V_2 then ensures the uniqueness of $\xi(z)$. In addition, $\xi(z)$ converges towards ϵ_s as z approaches $-\infty$. Furthermore, in the region $z>0$ (see Fig. 1) where $\epsilon(z)=1$, the acceptable solution of the Poisson equation is proportional to $V_1(z)=\exp(-kz)$. From Eq. (3.3), $\xi(z)$ is then equal to -1 throughout the vacuum region. Hence, Eq. (2.14) appears as a matching condition of $\xi(z)$ at the surface: The nonretarded eigenmodes of the system are such that $\xi(\mathbf{k},\omega,z)$ is a continuous function of z throughout space.

Consider now a periodic z dependence of $\epsilon(z)$ as an idealized model of a periodically compositionally modulated structure. According to Floquet theorem,[16] the Poisson equation (3.2) then has a pseudoperiodic solution of the form

$$V_1(z)=\exp(\mu_1 z)\cdot y_1(z) ,$$

where $y_1(z)$ has the period of $\epsilon(z)$, μ_1 being a complex number. In addition, when μ_1 is different from 0 or $\pm i\pi/L$, L denoting the period, a second independent pseudoperiodic solution exists,

$$V_2(z)=\exp(\mu_2 z)\cdot y_2(z) ,$$

y_2 being a periodic function of z, and $\mu_1+\mu_2=0$ (or equal to any integer multiple of $2i\pi/L$). Assuming $\mathrm{Re}\mu_1>0$, V_1 is the minimal solution of Poisson's equation and ξ, according to Eq. (3.3), is a periodic function of z, with period L, given by

$$\xi(z)=\frac{\epsilon(z)}{k}\frac{1}{y_1(z)}\left[\mu_1+\frac{dy_1(z)}{dz}\right] . \tag{3.4}$$

When $\mathrm{Re}\mu_1=0$ (hence, $\mathrm{Re}\mu_2=0$), $\xi(z)$ is no longer uniquely defined since the potential $V(z)$, as linear combination of V_1 and V_2, depends on two arbitrary constants. Consequently, and in absence of any external excitation, it is always possible to satisfy the boundary conditions at the surface [namely, by matching $V(z)$ and its derivative at the surface with the exponential solution of the Laplace equation in vacuum]. The linear combinations of the two independent Bloch solutions V_1 and V_2 which satisfy these boundary conditions correspond to nonretarded eigenmodes of the periodic system. The existence of such undamped eigenmodes requires ϵ to be real and periodic. In addition, the Poisson equation in that case has two independent Bloch solutions only in some intervals of the wave number k. These intervals will be called the Bloch continua of the polarization potential. They give rise to continua of nonretarded eigenmodes, by opposition with the localized, Fuch-Kliewer modes given by Eq. (2.14).

Returning to the EELS classical spectrum [Eq. (2.15)], we now show how the difficulty arising from the apparent nonuniqueness of the effective dielectric constant ξ_0 can be removed in the Bloch continua. By contrast with the hypothesis considered in the above discussion, the materials used in practice are characterized by complex dielectric constants. Hence, assuming a positive imaginary part in $\epsilon(z)$, Bloch solutions corresponding to $\mathrm{Re}\mu_1=\mathrm{Re}\mu_2=0$ do not exist, from a strict mathematical point of view. ξ is then uniquely defined, since V_2 is a divergent solution at $z=-\infty$ for any value of k, and $\xi(z)$ is the (complex) periodic function given by Eq. (3.4). This remains true even for vanishingly small dampings in $\epsilon(z)$. Hence, taking the limit $\mathrm{Im}\epsilon\to 0$, so as to reproduce a real periodic function $\epsilon(z)$,$\xi(z)$, as the limit of Eq. (3.4), will still be a periodic function of z. One can argue that, after the limit process has been performed, two periodic expressions for ξ could be obtained in the Bloch continua, depending on which Bloch solution V_1 or V_2 is considered. In fact the two periodic expressions for $\xi(z)$ are complex conjugate of each other, and one must select the solution so as to obtain $\mathrm{Im}\xi_0>0$. This choice ensures the positive definiteness of the classical loss distribution $P_{\mathrm{cl}}(\omega)$. (Notice that arguments are presented in the next section to show that $\mathrm{Im}[-1/(\xi_0+1)]>0$ when $\mathrm{Im}\epsilon(z)>0$, even for a vanishingly small imaginary part in $\epsilon(z)$.) In conclusion, $\xi(z)$ is periodic and uniquely defined (so is ξ_0) when $\epsilon(z)$ is a periodic function of z, even in the Bloch continua which may arise when $\mathrm{Im}\epsilon(z)=0$, provided one regards this idealized situation as a limiting process by considering vanishingly small dampings in the dielectric constant.

B. Riccati equation for ξ

Taking the derivative of both members of Eq. (3.1) with respect to z, and due to the Poisson equation, the following Riccati equation is obtained for ξ:

$$\frac{1}{k}\frac{d\xi(z)}{dz}+\frac{\xi^2(z)}{\epsilon(z)}=\epsilon(z) . \tag{3.5}$$

By integrating this differential equation, it is thus possible to deduce the effective dielectric function $\xi_0=\xi(0)$ of the medium without recourse to the Poisson equation. When solving Eq. (3.5), we have to impose a suitable boundary condition, according to the above discussion. For, if $\epsilon(z)$ assumes a constant asymptotic value ϵ_s when z approaches $-\infty$, we impose that $\lim\xi(z)=\epsilon_s$, so as to obtain the solution (3.3). (In addition, this method is well conditioned from the numerical point of view: It is very similar to the Miller backward algorithm used to solve difference equations.[17]) When $\epsilon(z)$ is a periodic function of z, one looks for a periodic solution of Eq. (3.5). Hence, the boundary condition to impose in such a case is $\xi(0)=\xi(-L)$, L being the period. If, in addition, $\epsilon(z)$ is real, Eq. (3.5) does not have a real periodic solution in the Bloch continua, if any, as explained above. One, thus, has to allow $\epsilon(z)$ to be complex, and look for the solution with a positive imaginary part at $z=0$. Outside the Bloch continua, however, a real periodic solution exists [the conditions of existence of periodic solution(s) for Riccati equations have been considered in specialized literature[18]].

Suppose the solution of the Riccati equation has been computed. Then, a straightforward integration of Eq. (3.1) yields the following expression for the potential:

$$\ln[V(z)]=C+k\int\frac{\xi(z)}{\epsilon(z)}dz , \tag{3.6}$$

where C is an arbitrary integration constant. As a particular application of this result, consider the case of the periodic solution of the Riccati equation obtained when $\epsilon(z)$ is periodic. Owing to Eq. (3.6), the potential has the pseudoperiodic form $V(z-L)=\sigma V(z)$, where the periodicity factor σ is given by

$$\sigma=\exp\left[k\int_0^{-L}\frac{\xi(z)}{\epsilon(z)}dz\right] . \tag{3.7}$$

We return to this result in Sec. V.

C. Asymptotic solutions

Asymptotic solutions of the Riccati equation for small or large values of k are easy to obtain by standard perturbation methods. Let us restrict attention to periodic $\epsilon(z)$ and look for the asymptotic solution of the Riccati equation (3.5) when $k\to 0$. As a result of such an analysis, conditions for existence of Bloch continua at $k=0$ will be deduced. To this end, let us develop ξ in Taylor series in a neighborhood of $k=0$:

$$\xi=\xi^{(0)}+\xi^{(1)}k+\xi^{(2)}k^2/2+\ldots . \tag{3.8}$$

Inserting this development in the Riccati equation yields the following results:

$$\xi^{(0)}=C_0 , \tag{3.9}$$

$$\xi^{(1)}=C_1+\int_0^z \epsilon(x)dx - C_0^2 \int_0^z [1/\epsilon(x)]dx , \tag{3.10}$$

where C_0 and C_1 are arbitrary integration constants. As $\xi(z)$ is a periodic function of z for any value of k, the coefficients $\xi^{(i)}$ of the development (3.8) must be a periodic function of z, with the period L of the superlattice. Imposing the periodicity of $\xi^{(1)}$ allows us to determine C_0, next C_1 is obtained by requiring that $\xi^{(2)}$ is periodic, and so on. The following result is obtained for C_0, which corresponds to the limit of ξ for vanishingly small k:

$$C_0=\pm\left[\frac{\int_0^{-L}\epsilon(z)dz}{\int_0^{-L}[1/\epsilon(z)]dz}\right]^{1/2} . \tag{3.11}$$

The sign in the above expression must be chosen so as to lead to a physical value for the periodicity factor σ [Eq. (3.7)], i.e., $|\sigma|\leq 1$, and thus avoid exponentially increasing polarization potential for small k. When $\epsilon(z)$ is real, Eq. (3.11) immediately shows that Bloch solutions exist at $k=0$ only for $\epsilon(z)$ functions such that nonreal values are obtained for C_0. A necessary condition for this to occur is that $\epsilon(z)$ changes sign in the period.

The $k=0$ limit C_0 of ξ can be interpreted as the effective dielectric function of a uniaxial crystal with its c axis perpendicular to the surface, the (macroscopic) anisotropy of the superlattice being due to the succession of periods in the z direction. For such a semi-infinite anisotropic material, indeed, it has been shown[5] that ξ equals $(\epsilon_{\parallel}\epsilon_{\perp})^{1/2}$, where $\epsilon_{\parallel}$ and $\epsilon_{\perp}$ are the dielectric tensor components in the crystal principal axes. As k approaches 0, the effective dielectric components $\epsilon_{\parallel}$ and $\epsilon_{\perp}$ of the superlattice reduce to $1/\langle\epsilon^{-1}\rangle_{\rm av}$ and $\langle\epsilon\rangle_{\rm av}$, where the symbols $\langle\ \rangle_{\rm av}$ denotes the average over the period L of the system.[19] Equation (3.11) then follows from these results, which can easily be retrieved by expressing the equivalent capacitance of series and parallel combinations of capacitors.

Consider now the case of large k. Although this asymptotic situation is irrelevant as far as EELS is concerned (due to the aperture cutoff $k_{\rm max}$), it gives some insight into the short-wavelength behavior of the effective dielectric function ξ_0. Ignoring the obvious limitations of the present macroscopic theory as $1/k$ becomes comparable with the interatomic distances, and assuming that $\epsilon(z)$ is differentiable with respect to z, one obtains the following asymptotic development:

$$\xi(z)=\epsilon(z)-\frac{d\epsilon}{dz}\frac{1}{2k}+\left[2\epsilon\frac{d^2\epsilon}{dz^2}-\left[\frac{d\epsilon}{dz}\right]^2\right]/\epsilon\frac{1}{8k^2}+\dots . \tag{3.12}$$

This equation indicates that the effective dielectric function ξ_0 for large k is intimately related to the behavior of the dielectric constant in the immediate neighborhood of the surface ($z=0$). It also shows that, for real periodic and differentiable $\epsilon(z)$ functions, Bloch continua do not exist at $k=\infty$, since the limit for large k of $\epsilon(z)$ would identify with $\epsilon(z)$ and would be real in that case.

IV. MULTILAYERED MATERIALS

In this section we will be concerned with heterogeneous materials made of a succession of layers with parallel interfaces. The simplest example of such planar stratified material is a single film deposited on a substrate. The synthesized superlattices considered in the next section also belong to this class of materials. Basically, we have to solve the Riccati equation (3.5) so as to determine the effective dielectric function ξ_0 of the system, from which the energy-loss spectrum can be deduced. To do this, a model of the dielectric constant profile $\epsilon(\omega,z)$ in multilayered materials is required.

As far as EELS is concerned, rapid spatial variations of $\epsilon(z)$ are irrelevant because the k integration in Eq. (2.15) is restricted to small values of the wave vector $\mathbf{k}$. Indeed, spatial variations of $\epsilon(z)$ occuring over regions of z much smaller than $1/k_{\rm max}$ are actually smoothed out when solving the Riccati equation (refer to the power expansion [Eqs. (3.8)—(3.11)] of $\xi(z)$). Hence, the knowledge of the exact variations of $\epsilon(z)$ near the interfaces is irrelevant in the present macroscopic theory, provided these variations take place over widths much smaller than $1/k_{\rm max}$. Consequently, it is not too crude an approximation to consider abrupt variations of $\epsilon(z)$ at the interfaces, especially in the multilayered materials with sharp interfaces. By contrast, slow spatial variations of $\epsilon(z)$ are relevant in EELS and could effectively be taken into account by solving numerically Eq. (3.5). As a simplifying assumption, however, we will assume that $\epsilon(z)$ takes constant values in each layer. In so doing, an analytical expression for the effective dielectric constant $\xi_0(k,\omega)$ will be obtained, as we now show.

This section is, thus, aimed at solving the Riccati equation for a histogramlike profile of $\epsilon(\omega,z)$. In the following, the thicknesses of the layers $i=1,2,3,\dots$, will be denoted by d_i which, together with the dielectric constants ϵ_i—and their ω dependence—characterizing the materials which the layers are made of, constitute the input of the Riccati equation. The general solution of that equation for a constant ϵ is

$$\xi(z)=\epsilon\frac{C+\epsilon\tanh(kz)}{\epsilon+C\tanh(kz)} , \tag{4.1}$$

where C is an arbitrary integration constant; the solution of the Riccati equation in layer i can obviously be written as

$$\xi(z)=\epsilon_i\frac{\xi_i+\epsilon_i\tanh[k(z-z_i)]}{\epsilon_i+\xi_i\tanh[k(z-z_i)]},\quad z_i\leq z\leq z_{i-1} . \tag{4.2}$$

In this equation, ξ_i denotes the value of $\xi(z_i)$ at the lower end z_i of the layer. By setting $z=z_{i-1}$ in Eq. (4.2), we obtain the following expression for ξ_{i-1} at the upper end z_{i-1}:

$$\xi_{i-1}=\xi(z_{i-1})=\epsilon_i\coth(kd_i)-\frac{[\epsilon_i/\sinh(kd_i)]^2}{\epsilon_i\coth(kd_i)+\xi_i} . \tag{4.3}$$

Repeating this treatment in each layer, and since $\xi(z)$ is a continuous function of z, by construction (in other words, ξ_i takes the same value when computed from above and

from below the interface i), we obtain the following continued-fraction expansion of ξ_0, i.e., the effective dielectric function of the stratified material:

$$\xi_0=a_1-\cfrac{b_1^2}{a_1+a_2-\cfrac{b_2^2}{a_2+a_3-\cfrac{b_3^2}{a_3+a_4-\cdots}}}, \quad (4.4)$$

where we have used the notations

$$a_i=\epsilon_i \coth(kd_i) , \quad (4.5)$$

$$b_i=\epsilon_i/\sinh(kd_i) . \quad (4.6)$$

The analysis of the continued fraction (4.4) yields the following results. When the ϵ_i assume positive imaginary parts, $1/(\xi_0+1)$ is a so-called positive-definite continued fraction.[20] Among the consequences of this property, we note that ξ_0 has a positive imaginary part. Hence, the loss function $\mathrm{Im}[-1/(\xi_0+1)]$ [refer to Eq. (2.15)] is positive. Let us remark that the continued-fraction expansion (4.4) can still be used for any z dependence of $\epsilon(\omega,z)$ by approximating the actual profile by a histogram. As it is always possible to approximate, to any degree of accuracy, any bounded function by such a histogram, we conclude that the positive definiteness of $\mathrm{Im}\xi_0$, as solution of the Riccati equation, is quite general.

When the number n of layers is finite, and when such a heterogeneous film has been deposited onto a semi-infinite substrate (the "substrate" could be the vacuum in the case of self-supporting films), the continued fraction (4.4) terminates. Indeed, by allowing the thickness d_{n+1} of the substrate to be infinity (in practice, large with respect to $1/k$), Eq. (4.6) yields $b_{n+1}=0$. Explicit expressions for ξ_0 can then be obtained for small values of n, for instance

$$\xi_0=\epsilon_s, \quad n=0 \quad (4.7)$$

$$\xi_0=\epsilon_1\frac{\epsilon_1\tanh(kd_1)+\epsilon_s}{\epsilon_s\tanh(kd_1)+\epsilon_1}, \quad n=1 \quad (4.8)$$

$$\xi_0=\epsilon_1\frac{\epsilon_1\tanh(kd_1)[\epsilon_2+\epsilon_s\tanh(kd_2)]+\epsilon_2[\epsilon_s+\epsilon_2\tanh(kd_2)]}{\epsilon_2\tanh(kd_1)[\epsilon_s+\epsilon_2\tanh(kd_2)]+\epsilon_1[\epsilon_2+\epsilon_s\tanh(kd_2)]}, \quad n=2 . \quad (4.9)$$

Such analytical formulas rapidly become cumbersome as n increases. Thus, it is preferable to use the continued-fraction-expansion (4.4), an object which is easy to deal with on a (micro)computer.

V. SUPERLATTICES

Superlattices built with two different materials are considered here as semi-infinite multilayers where the sequence formed from two layers 1 and 2 is repeated periodically. By definition, the layer in contact with the vacuum is made of material 1.

In this idealized situation, the continued fraction (4.4) itself becomes periodic, and its limit can be evaluated analytically.[20] The theory of periodic continued fractions leads to the following quadratic equation:

$$(a_1+a_2)\xi_0^2-(\epsilon_1^2-\epsilon_2^2)\xi_0-(a_2\epsilon_1^2+a_1\epsilon_2^2)=0 . \quad (5.1)$$

When writing the two solutions of this equation,

$$\xi_0=\frac{\epsilon_1^2-\epsilon_2^2}{2(a_1+a_2)} \pm\left[\left[\frac{\epsilon_1^2-\epsilon_2^2}{2(a_1+a_2)}\right]^2+\frac{a_2\epsilon_1^2+a_1\epsilon_2^2}{a_1+a_2}\right]^{1/2}, \quad (5.2)$$

the physically acceptable ξ_0 is the solution closest to the first approximant $a_1-b_1^2/(a_1+a_2)$ of the continued fraction.

Once ξ_0 has been computed, the periodicity factor σ of the polarization potential can be deduced (refer to Sec. III B). Indeed, it is easy to perform analytically the z integration in Eq. (3.7), to obtain

$$\sigma=\frac{(a_1-\xi_0)/b_1}{(a_2+\xi_0)/b_2} . \quad (5.3)$$

From this result, it is not difficult to prove that the correct sign for ξ_0 in Eq. (5.2), as determined according to the criterion mentioned above, ensures that the modulus of σ is smaller than unity and hence that we have chosen the physical solution of the Poisson equation, namely, that solution which decreases exponentially when one proceeds into the superlattice.

The calculations of the EELS spectra presented below have been performed using realistic dampings in the $\epsilon_i(\omega)$. However, the analysis of the results can be made more transparent if the dielectric constants are regarded as real, the dampings actually being small quantities. Hence, we now regard Eq. (5.1) as a quadratic equation with real coefficients. As a solution of that equation, ξ_0 can assume real as well as complex values. From Eq. (5.3), one concludes that real values of ξ_0 are related to an exponentially decaying potential. For instance the Fuchs-Kliewer surface modes of the superlattice correspond to $\xi_0=-1$. These modes play an important role in the theory of EELS, as explained in Sec. II, since they give rise to a macroscopic polarization field outside the material and are thus responsible for strong energy losses of the electron. In the (ϵ_1,ϵ_2) plane, Eq. (5.1) has a root equal to -1

along the curve of the equation

$$[1+\epsilon_1 \coth(kd_1)](1-\epsilon_2^2) - [1-\epsilon_2 \coth(kd_2)](1-\epsilon_1^2)=0 . \quad (5.4)$$

However, a further discussion is needed to select the pieces of the above cubical hyperbola which actually correspond to the Fuchs-Kliewer modes of the system, notwithstanding the choice of the correct sign for ξ_0 in Eq. (5.2). The results are illustrated in Fig. 2 for two ratios of the layer thicknesses d_1 and d_2 of the superlattice. Notice that the existence of Fuchs-Kliewer modes requires ϵ_1 or ϵ_2 to be negative.

For values of the parameters such that Eq. (5.1) presents two complex conjugate solutions, the continued fraction (4.4) (with assumed real coefficients) does not converge. This phenomenon, already discussed in Sec. III, is intimately connected with the existence of two independent Bloch solutions for the polarization potential corresponding to the two solutions of the quadratic equation (5.1). In fact, these two solutions are equally distant from the first approximant of the continued fraction so that the proper sign in Eq. (5.2) can no longer be determined. However, we are still allowed to make use of Eq. (5.2) in the Bloch regions, provided one considers the idealized situation of real ϵ_i as the limit already discussed of vanishingly small dampings in the dielectric constants. In these conditions, the solution which has a positive imaginary part must be retained for ξ_0.

The regions of the parameters where Bloch modes exist have been represented by shaded areas in Fig. 2. These regions are bounded by the straight lines of the equation $\epsilon_1+a\epsilon_2=0$, $\epsilon_2+a\epsilon_1=0$, $\epsilon_1+b\epsilon_2=0$, and $\epsilon_2+b\epsilon_1=0$, where

$$a=\tanh(kd_1/2)\tanh(kd_2/2) \quad (5.5)$$

and

$$b=\tanh(kd_1/2)/\tanh(kd_2/2) . \quad (5.6)$$

Note that the gaps which separate the Bloch continua (see Fig. 2) disappear when the thicknesses d_1 and d_2 of the alternating layers coincide, since $b=1$ [Eq. (5.6)] in that limiting case.

The above discussion was quite general in the sense that it did not rely on any specific ω dependence of the dielectric constants. We now turn our attention to superlattices made of polar semiconductors and explicitly make use of a Lorentzian model for the infrared dielectric constant of such materials, namely,

$$\epsilon(\omega)=\epsilon_\infty+\frac{(\epsilon_0-\epsilon_\infty)\omega_{TO}^2}{\omega_{TO}^2-\omega^2-i\gamma\omega} . \quad (5.7)$$

As for the parameters involved in this expression, we have primarily made use of data tabulated by Frederikse.[21] It now becomes easy to evaluate the loss function

$$\mathrm{Im}\{-1/[\xi_0(k,\omega)+1]\}$$

using Eq. (5.2). The results are shown in Fig. 3, where

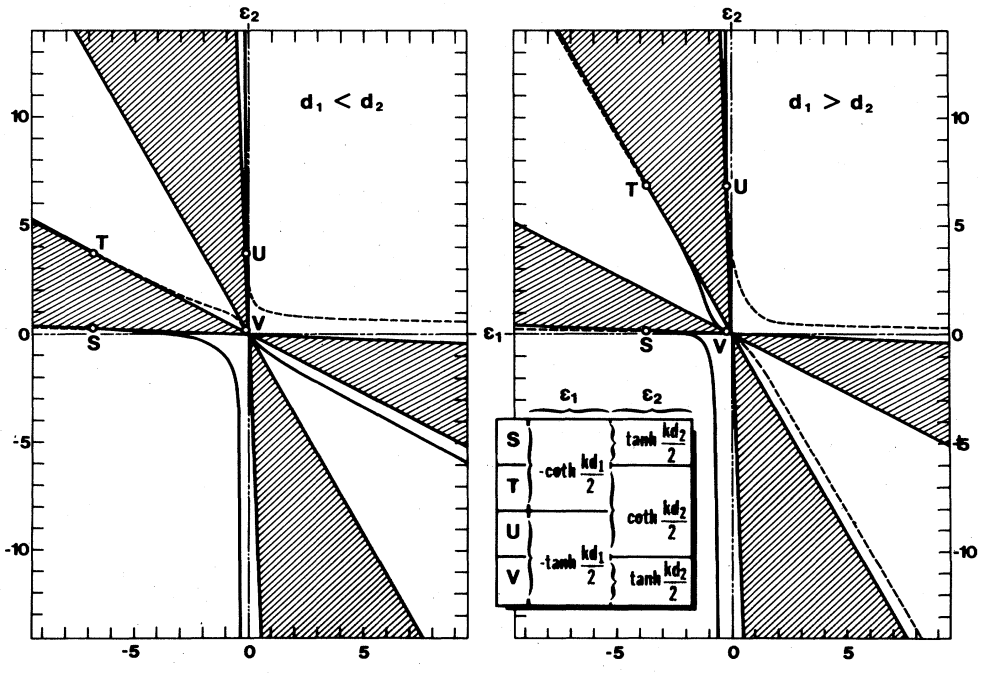

FIG. 2. Algebraic analysis of Eq. (5.1) is summarized in this figure in the (ϵ_1,ϵ_2) plane for a selected value of k. The (assumed real) dielectric constants of the two layers which the superlattice is made of are considered as independent parameters. The shaded areas correspond to regions where ξ_0 takes complex values, and are related to Bloch modes of the polarization potential. The curves (solid lines) represent the localized Fuchs-Kliewer modes ($\xi_0=-1$). For convenience, the dashed lines have been represented so as to illustrate the complete cubical hyperbola [Eq. (5.4)]. Remark that the localized branches split off the continua at the points S—V where the cubical hyperbola is tangent to the boundaries of the continua. The coordinates of these points are given in the figure.

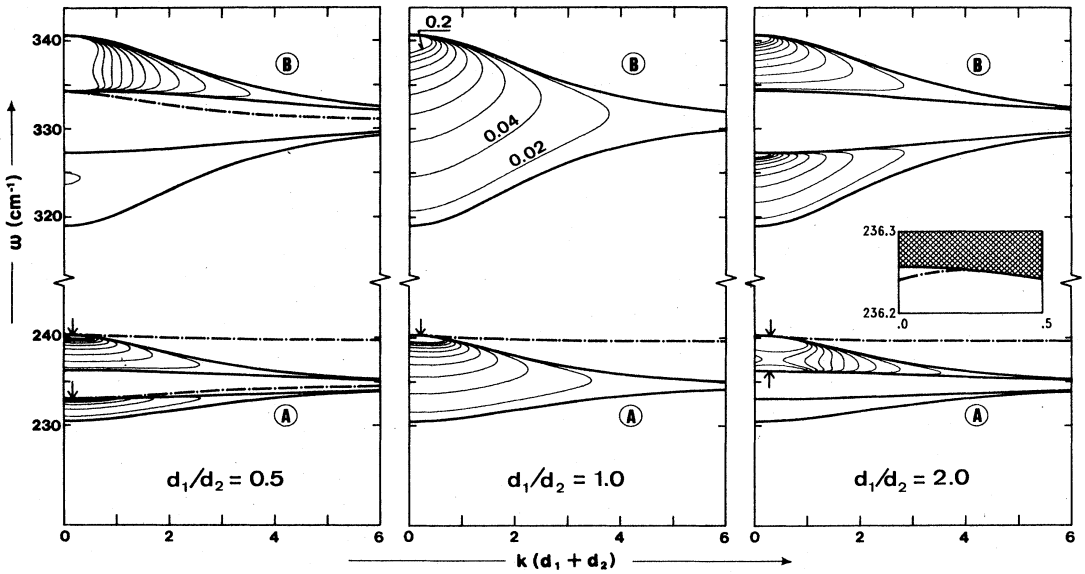

FIG. 3. Contour plots of the loss function $\mathrm{Im}\{-1/[\xi_0(k,\omega)+1]\}$ related to three GaSb-AlSb superlattices with various layer thicknesses. The contour curves range from $\mathrm{Im}[-1/(\xi_0+1)]=0$ (heavy lines, representing the borders of the Bloch continua) to 0.2, by equidistant steps equal to 0.02. The absence of contour curves in some continua indicates that the loss function assumes very small values in these continua. Real Lorentzian shapes have been assumed for the two dielectric constants $\epsilon_i(\omega)$ [Eq. (5.7)]. In units of cm^{-1}, the related TO and LO frequencies are $\omega_{\mathrm{TO}}=230.5$, $\omega_{\mathrm{LO}}=240.3$ for the first layer (GaSb), and $\omega_{\mathrm{TO}}=319.0$, $\omega_{\mathrm{LO}}=340.6$ for the second layer (AlSb). In the figure, the dot-dashed curves represent the localized Fuchs-Kliewer modes of the system, which correspond to isolated poles of the loss function. When present, the arrows indicate where the localized branches enter the continua. The gap mode in region A (see the text) for $d_1/d_2=2$ is shown in the detailed portion of the figure where the shaded area corresponds to the high-frequency Bloch continuum of region A.

contour plots of the loss function have been represented for models of GaSb-AlSb superlattice, a recently built heterostructure.[22] Assuming again real dielectric constants as deduced from Eq. (5.7) by setting the dampings γ_i equal to zero, Bloch modes exist only at frequencies ω such that the dielectric constants $\epsilon_1(\omega)$ and $\epsilon_2(\omega)$ have opposite signs (refer to Fig. 2). In the following, we denote by A the ω domain where $\epsilon_1(\omega)<0$ and $\epsilon_2(\omega)>0$, while B corresponds to $\epsilon_2(\omega)<0$ and $\epsilon_1(\omega)>0$.

The loss function vanishes outside the Bloch continua, except along the localized Fuchs-Kliewer branches where it has isolated poles. In region A (the low-frequency portion of Fig. 3—although the position of region A with respect to B is irrelevant for our discussion), a localized mode exists for any ratio of the thicknesses d_1 and d_2. This mode splits off the A Bloch continuum at a nonzero value of k. As k increases, this mode converges towards the frequency of the surface phonons of the first layer, i.e., to the frequency such that $\epsilon_1(\omega)=-1$.

When the first layer is thinner than the second ($d_1<d_2$), Fuchs-Kliewer localized modes also exist in the gaps which separate the Bloch continua in regions A and B. In region B, the gap mode exists at $k=0$; by contrast, the gap mode in region A enters a Bloch continuum at a nonzero value of k. As k increases, the gap modes converge toward the frequencies of the interfacial phonons, such that $\epsilon_1(\omega)+\epsilon_2(\omega)=0$. This result is intimately connected with our assumption of a histogramlike z dependence for $\epsilon(\omega,z)$. Indeed, Eq. (3.12) shows that the limit of $\xi_0(k,\omega)$ as k approaches infinity should coincide with the value of $\epsilon(\omega,0)$ at the surface $z=0$. In our case, however, $\epsilon(\omega,z)$ is not differentiable with respect to z. In fact, the large-k limit of $\xi_0(k,\omega)$ is undetermined at the frequencies such that $\epsilon_1(\omega)+\epsilon_2(\omega)=0$. This explains why the gap modes, and the Bloch continua as well, converge towards these frequencies. These behaviors should not be extrapolated to arbitrarily large values of k, as the theory of large-k phonons in superlattice requires detailed microscopic treatments.[23] Finally, Fig. 3 indicates that the gap mode in the region B disappears when $d_1>d_2$. The mode in the other gap (refer to the detailed portion of the figure) is somewhat complementary to what was observed in region A when $d_1<d_2$: In the former case, the gap mode exists for small k values and enters into the Bloch region at a finite value of k.

Figure 4 shows the polarization potential which has been computed for the GaSb-AlSb superlattice with $d_1/d_2=\frac{1}{2}$, at the frequencies corresponding to the three localized eigenmodes of Fig. 3 for a wave number k equal to $2.3/(d_1+d_2)$. For the three modes, the envelope of the potential decreases exponentially away from the surface of the superlattice. Figure 4 clearly indicates a strong distinction between the two gap modes, on the one hand, and the mode located above the continua of region A, on the other hand. While the potential related to the latter mode rapidly vanishes as one proceeds into the material, the extent of the potential corresponding to the two gap modes is several periods.

While the localized Fuchs-Kliewer modes correspond to isolated poles of the loss function, the Bloch continua ap-

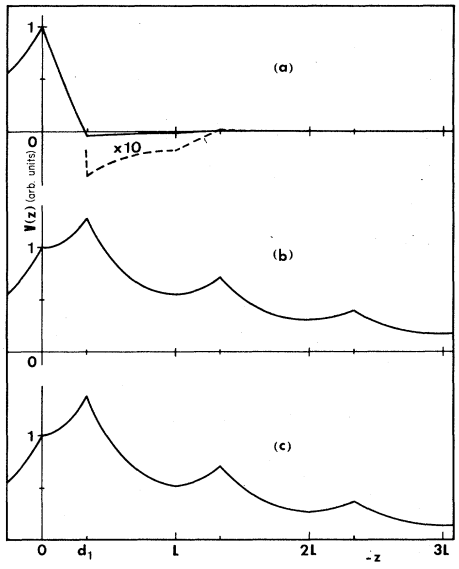

FIG. 4. Polarization potential corresponding to the three localized eigenmodes of the GaSb-AlSb superlattice considered in Fig. 3 for $d_1/d_2=\frac{1}{2}$. The wave number used for these calculations is $k=2.3/L$, where $L=d_1+d_2$ is the period of the superlattice. The related frequencies ω of the three eigenmodes are (a) 239.9 cm^{-1}, (b) 233.8 cm^{-1}, and (c) 332.5 cm^{-1}. Part (a) of the figure is for the localized mode located above the continua of region A (Fig. 3). The periodicity factor of this potential [Eqs. (3.7) and (5.3)] has been found equal to -0.018 (the potential changes its sign in each period). The curves (b) and (c) correspond to the gap modes of regions A and B, respectively; the related periodicity factors are 0.55 and 0.52. By contrast, the potential in the vacuum region (left-hand side of the figure) decreases by a factor 10 ($e^{-2.3}$) as the distance from the surface increases by steps equal to the period L of the superlattice.

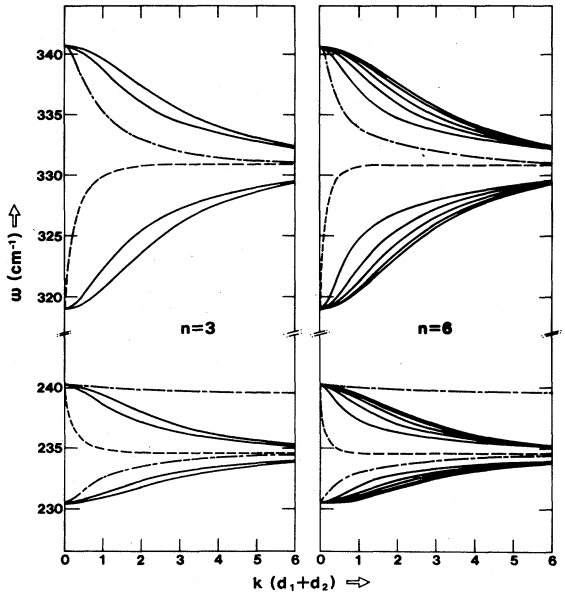

FIG. 5. Most of the Fuchs-Kliewer interface modes of a superlattice with a finite number n of period accumulate in some regions of the (k,ω) plane as n increases (solid curves). At the limit of infinite n, these regions give rise to Bloch continua. For these calculations, we have considered two GaSb-AlSb/GaSb superlattices formed from n periods deposited onto a semi-infinite GaSb substrate. The parameters for the dielectric constants ϵ_1 and ϵ_2 are those used for Fig. 3, and the thickness ratio d_1/d_2 equals $\frac{1}{2}$. The dashed curves correspond to modes that we attribute to the interface with the semi-infinite substrate; the weight of these modes vanishes for large values of n. The dot-dashed curves clearly converge towards the localized Fuchs-Kliewer modes of the semi-infinite superlattice as n approaches infinity (refer to Fig. 3).

pear as regions where the frequencies of interacting Fuchs-Kliewer interface modes accumulate as the number of periods progressively increases. This is clearly evidenced in Fig. 5 which displays the Fuchs-Kliewer modes for a system formed from n periods made of GaSb and AlSb layers, and deposited onto a semi-infinite GaSb substrate. This system presents $4n+1$ modes resulting from $2n$ GaSb/AlSb interfaces and the GaSb/vacuum interface. In semi-infinite superlattices ($n\rightarrow\infty$), instead of isolated poles of the loss function, we actually observe a continuous series of poles in the Bloch regions [i.e., a cut of $-1/(\xi_0+1)$ as a function of k at a given frequency ω]. A continuous series of modes exist in these regions with a nonvanishing polarization field outside the superlattice, as explained above. Note that bulk modes also exist in multilayered materials (at frequencies such that the dielectric constant of one layer or the other vanishes). However, these bulk modes do not generate a polarization field outside the material and, for that reason, cannot be detected by EELS in the reflection geometry.

VI. THEORETICAL EELS SPECTRA AT THE SURFACE OF A SUPERLATTICE

We now consider the computation of EELS spectra of a superlattice. The results presented in this section have been obtained using the Lorentzian expression (5.7) for the dielectric constants where realistic dampings have been introduced ($\gamma/\omega_{TO}\approx 0.01$). Small imaginary parts in the ϵ_i's have only small effects: The loss function $\mathrm{Im}[-1/(\xi_0+1)]$ assumes nonzero values inside the Bloch continua, as before, but the boundaries of the continua are now diffuse rather than sharp; the loss function is very small outside these regions except in the immediate neighborhood of the localized branches, where it takes large values. Hence, the structures of the EELS classical spectra shown in Fig. 6 are easy to understand. These spectra correspond to the GaSb-AlSb superlattices considered in Fig. 3. The low-frequency, strong δ-like peak in both panels of Fig. 6 has its origin in the localized Fuchs-Kliewer mode above the Bloch continua in the region A (refer to Fig. 3). Furthermore, the modes localized in the gaps of both regions A and B when $d_1<d_2$ are responsible for two other peaks ($\omega=233$ and 333 cm^{-1}), somewhat less intense than the former. When $d_1>d_2$, the high-frequency part of the spectrum is attributed to the Bloch modes only, as there is no gap mode in the region B for such a superlattice. As for region A, the localized gap mode, and the upper Bloch continuum as well, are responsible for the structure observed in the low-frequency wing of the main EELS peak.

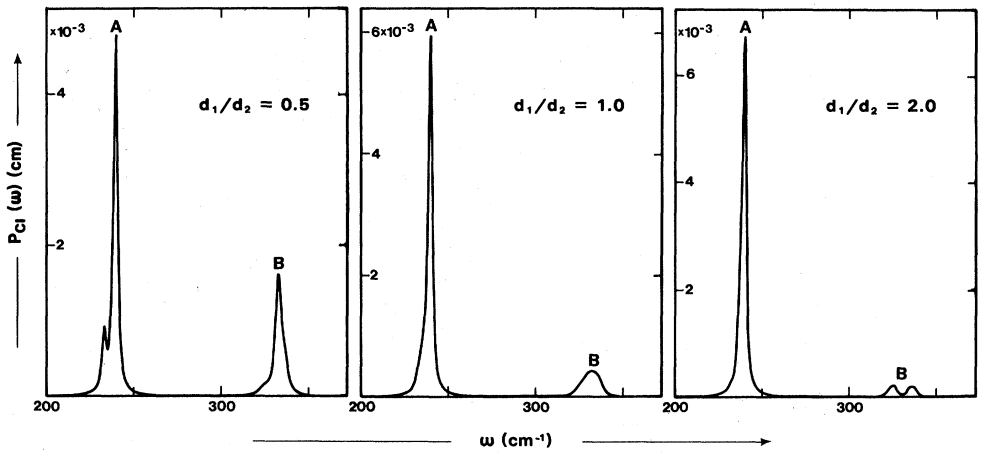

FIG. 6. Classical EELS spectrum $P_{cl}(\omega)$ for the GaSb-AlSb superlattices already considered in Fig. 3. The period d_1+d_2 of the three superlattices is equal to 300 Å. Calculations were carried out for a 5-eV specularly reflected electron under an incidence $\psi_i=70°$. The half-acceptance angle of the detector is 1.8°.

As an illustrative example, Fig. 7 shows the full EELS spectra of the GaSb-AlSb superlattice with $d_1=100$ Å and $d_2=200$ Å. This spectrum has been computed as explained in Sec. II [Eqs. (2.3)—(2.5)] for a temperature $T=300$ K. The spectrum has further been broadened by convolution with a Lorentzian response function, the width of which is 30 cm^{-1}, so as to simulate a finite experimental resolution. The two small peaks in the interval 200—400 cm^{-1} corresponds to the classical loss distribution. Of course, the structure of the A peak (see Fig. 6) has been washed out due to the simulated poor resolution of the spectrum. The two-peak structure in the $\omega<0$ region of Fig. 7 is the gain replica of the classical spectrum $P_{cl}(\omega)$.

The classical loss distributions of Fig. 8 have been computed first, for a GaSb(first layer)-AlSb superlattice and next, for AlSb(first layer)-GaSb. The purpose of these calculations is to evidence the effects of the first layer on the EELS spectrum of a superlattice. The thicknesses of the layers, d(GaSb)=50 Å and d(AlSb)=100 Å, are identical in both systems, as if the topmost layer of one superlattice were removed so as to define the second superlattice. Hence, in addition to the effects resulting from the permutation of the layers, the differences between the two spectra of Fig. 8 is further amplified by the fact that the d_1/d_2 ratio, from $\frac{1}{2}$ in Fig. 8(a), grows into 2 in Fig. 8(b). On the other hand, the period of the GaSb-AlSb superlattice being half the period of the superlattice with $d_1/d_2=\frac{1}{2}$ already considered explains the differences between the spectra of Fig. 6 and Fig. 8(a): In the latter case, the A and B peaks have nearly equal intensities.

We now turn our attention to another, extensively studied, superlattice made of GaSb and InAs,[10] for which the layer thicknesses that we have chosen are below the semiconductor-semimetal transition.[24] As far as macroscopic vibrational properties are concerned, the GaSb-

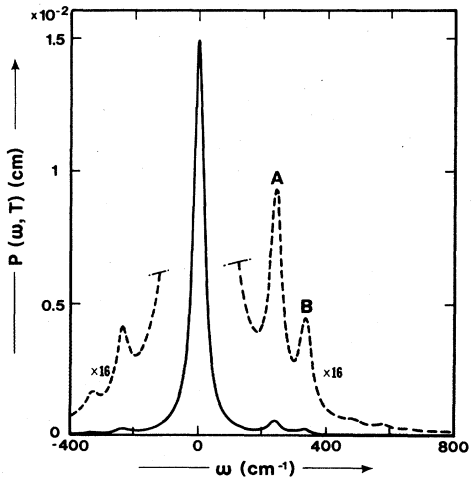

FIG. 7. Full EELS spectrum $P(\omega,T)$ for a GaSb-AlSb superlattice with d_1(GaSb)=100 Å and d_2(AlSb)=200 Å. The temperature T is 300 K. The simulated resolution which has been achieved by convoluting $P(\omega,T)$ with a Lorentzian function is 30 cm^{-1}.

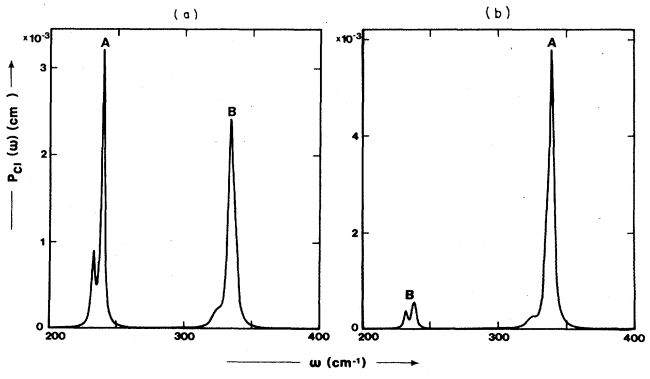

FIG. 8. Comparison of the EELS loss distribution $P_{cl}(\omega)$ for (a) GaSb(first layer)-AlSb and (b) AlSb(first layer)-GaSb. The layer thicknesses for both of these superlattices are d(GaSb)=50 Å and d(AlSb)=100 Å. The electron parameters for the simulated EELS experiment are those used for Fig. 6.

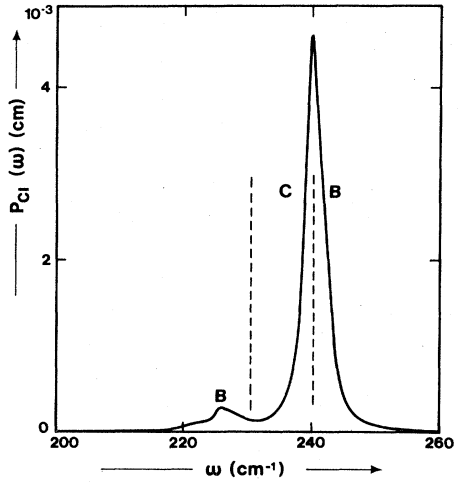

FIG. 9. Classical EELS loss distribution $P_{cl}(\omega)$ for a GaSb-InAs superlattice with $d_1=60$ Å and $d_2=80$ Å. The electron energy is 6 eV and the incidence angle is 45°. The dashed lines correspond to the ω_{TO} and ω_{LO} frequencies of GaSb (refer to the caption of Fig. 3). As for the second layer (InAs), $\omega_{TO}=219.0$, $\omega_{LO}=243.5$ cm^{-1}. The ω_{LO} frequencies are computed from the Lyddane-Sachs-Teller relation.

InAs semiconducting superlattice differs from the GaSb-AlSb heterostructure studied here above, and from the hypothetically thick GaAs-InAs superlattice considered previously,[8] in this sense that the Restsrahlen interval $(\omega_{TO},\omega_{LO})$ of the first layer (GaSb) is included inside the Restsrahlen of the second layer (InAs). Consequently, there is a ω region C where both $\mathrm{Re}\epsilon_1$ and $\mathrm{Re}\epsilon_2$ are negative, and the region C separates two regions B where $\mathrm{Re}\epsilon_2<0, \mathrm{Re}\epsilon_1>0$. These regions are indicated in Fig. 9, where the classical loss distribution is plotted. The position of the maximum of the main EELS peak (whose origin is the localized branch in the $\epsilon_1<0,\epsilon_2<0$ region of Fig. 3) corresponds to the frequency of the macroscopic surface phonon of GaSb, which lies on the high-frequency border of region C.

VII. CONCLUDING REMARKS

In this paper, emphasis has been put on the calculation of the effective dielectric function of multilayered materials, so as to deduce the EELS spectrum of such systems. The assumption of a histogramlike z dependence of the dielectric constant in an idealized multilayer is very convenient, for it leads to a simple continued fraction expansion of $\xi_0(k,\omega)$. This assumption is however not essential: In principle, the Riccati equation (3.5) allows us to deal with any model of $\epsilon(\omega,z)$. For instance, one could account for a nonabrupt spatial variation of the electron density in semimetallic or metallic heterostructures, and thus take account of the related high-multipole surface and interface plasma excitations,[25] although these modes are likely to play a minor role in the long-wavelength theory of EELS.

ACKNOWLEDGMENTS

This work is sponsored by the Ministry for Science Policy (Project IRIS) and by the Belgian National Science Foundation. The authors also acknowledge Paul Thiry and Michel Liehr for stimulating discussions.

APPENDIX

In this appendix, it is shown how the two-dimensional k integration in Eq. (2.15) can be reduced to a one-dimensional integration over k in the interval $(0,k_{max})$ when $\xi_0(\mathbf{k},\omega)$ does not depend on the polar angle ϕ of the wave vector $\mathbf{k}$ (this is realized for isotropic target materials). Using polar coordinates, the integration over the polar angle ϕ (which is measured from the direction $\mathbf{v}_{||}$ of the incident electron) can be expressed in terms of the integral

$$J=\int_{\Phi}^{\pi-\Phi}\frac{u^2}{[(1-e\cos\phi)^2+u^2]^2}d\phi\ , \tag{A1}$$

where e and u are two dimensionless quantities given by $e=kv_{||}/\omega$, $u=kv_{\perp}/\omega$, and $\Phi(0\le\Phi\le\pi/2)$ denotes a function of k obtained from the analytical expression (2.16) of the domain D. We now indicate how the integral (A1) can be evaluated. This integral is first rewritten as follows:

$$J=\frac{1}{2}\left[\frac{I}{u}-\frac{\partial I}{\partial u}\right], \tag{A2}$$

where

$$I=\int_{\Phi}^{\pi-\Phi}\frac{u}{(1-e\cos\phi)^2+u^2}d\phi=\mathrm{Im}R\,(1+iu)\ , \tag{A3}$$

with

$$R(z)=\int_{\Phi}^{\pi-\Phi}\frac{d\phi}{e\cos\phi-z}$$
$$=\frac{1}{i(z^2-e^2)^{1/2}}\ln\left[\frac{z\tan\Phi-i(z^2-e^2)^{1/2}}{z\tan\Phi+i(z^2-e^2)^{1/2}}\right]. \tag{A4}$$

$R(z)$ is an analytic function of the complex variable $z=1+iu$ outside a cut along the real axis which contains the interval $(-e\cos\Phi,+e\cos\Phi)$. Consequently, when z is outside the cut, we can write

$$\frac{\partial I}{\partial u}=\mathrm{Re}R'(1+iu)\ , \tag{A5}$$

with

$$R'(z)=\frac{dR(z)}{dz}=-\left[\frac{e^2\sin(2\Phi)}{z^2-e^2\cos^2\Phi}+zR(z)\right]\frac{1}{z^2-e^2}\ . \tag{A6}$$

For $\Phi=0$ (which is realized as long as the wave number k is smaller than $k_{max}\cos\psi_i$), these formulas yield

$$J=\frac{\pi}{4}\frac{(\rho_+ +\rho_-)^2-4}{[4-(\rho_+ -\rho_-)^2]^{1/2}} \times\frac{\rho_+^2+\rho_-^2-(\rho_+ -\rho_-)^2(\rho_+^2+\rho_-^2-\rho_+\rho_-)/4}{(\rho_+\rho_-)^3}, \quad \text{(A7)}$$

where

$$\rho_\pm=(u^2+(1\pm e)^2)^{1/2} .$$

When Φ differs from 0, rather than manipulating the cumbersome analytical expressions obtained by deriving the imaginary and real parts involved in the above formulation, it is easier to compute numerically $R(z)$ and $R'(z)$ from Eqs. (A4) and (A6) using complex arithmetics, and next deduce the numerical value of J [Eq. (A2)]. Evaluation of the EELS spectrum then requires only a one-dimensional integration over k, with substantial saving in computing time.

[1]M. Liehr, P. A. Thiry, J. J. Pireaux, and R. Caudano, J. Vac. Sci. Technol. A **2**, 1079 (1984); Phys. Rev. B **29**, 4824 (1984).

[2]A. A. Lucas and M. Sunjic, Prog. Surf. Sci. **2**, 75 (1972); Surf. Sci. **32**, 439 (1972).

[3]H. Ibach and D. L. Mills, *Electron Energy Loss Spectroscopy* (Academic, New York, 1982).

[4]A. A. Lucas, J. P. Vigneron, Ph. Lambin, P. A. Thiry, M. Liehr, J. J. Pireaux, and R. Caudano, in *Proceedings of the Sanibel Symposium, St. Augustine, 1985* [Int. J. Quantum Chem. (to be published)].

[5]A. A. Lucas and J. P. Vigneron, Solid State Commun. **49**, 327 (1984).

[6]J. P. Vigneron, A. A. Lucas, P. A. Thiry, M. Liehr, J. J. Pireaux, and R. Caudano, in *Proceedings of the 17th International Conference on the Physics of Semiconductor, San Francisco, 1984* (Springer-Verlag, Berlin, 1985), p. 209.

[7]H. Raether, *Excitation of Plasmons and Interband Transitions by Electrons* (Springer-Verlag, Berlin, 1980).

[8]A preliminary report of the present work has appeared in Ph. Lambin, J. P. Vigneron, and A. A. Lucas, Solid State Commun. **54**, 257 (1985).

[9]A. A. Lucas, Ph. Lambin, J. P. Vigneron, P. Thiry, M. Liehr, J. J. Pireaux, and R. Caudano (unpublished).

[10]L. Esaki, in *Recent Topics in Semiconductor Physics,* edited by H. Kamimura and Y. Toyozawa (World Scientific, Singapore, 1983), pp. 1–71; J. Phys. (Paris) Colloq. **45**, C5-3 (1984).

[11]R. E. Camley and D. L. Mills, Phys. Rev. B **29**, 1695 (1984).

[12]The electromagnetic properties of nonterminated periodic stratified media can be found, e.g., in S. M. Rytov, Zh. Eksp. Teor. Fiz. **29**, 605 (1955) [Sov. Phys.—JETP **2**, 466 (1956)].

[13]G. F. Giuliani and J. J. Quinn, Phys. Rev. Lett. **51**, 919 (1983); G. F. Giuliani, J. J. Quinn, and R. F. Wallis, J. Phys. (Paris) Colloq. **45**, C5-285 (1984).

[14]For another use of a similar effective quantity, see R. R. Gerhardts and K. Kempa, Phys. Rev. B **30**, 5704 (1984).

[15]E. Evans and D. L. Mills, Phys. Rev. B **5**, 4126 (1972).

[16]F. M. Arscott, *Periodic Differential Equations* (Pergamon, London, 1964).

[17]J. Wimp, *Computation with Recurrence Relations* (Pitman, Boston, 1984).

[18]D. A. Sanchez, SIAM J. Appl. Math. **17**, 957 (1969).

[19]C. Colvard, T. A. Gant, M. V. Klein, R. Merlin, R. Fischer, H. Morkoc, and A. C. Gossard, Phys. Rev. B **31**, 2080 (1985); See also D. E. Aspnes, Phys. Rev. B **25**, 1358 (1982).

[20]H. S. Wall, *Analytic Theory of Continued Fractions* (Chelsea, New York, 1973).

[21]H. P. R. Frederikse, in *Physics Vade Mecum,* edited by H. L. Anderson (AIP, New York, 1981), p. 288.

[22]P. Voisin, C. Delalande, M. Voos, L. L. Chang, A. Segmuller, C. A. Chang, and L. Esaki, Phys. Rev. B **30**, 2276 (1984).

[23]S. Yip and Y. Chang, Phys. Rev. B **30**, 7037 (1984) and references therein.

[24]L. Esaki, J. Cryst. Growth **52**, 227 (1981); Y. Guldner, Physica **117B** and **118B**, 735 (1983).

[25]J. J. Quinn, Solid State Commun. **52**, 607 (1984), and references therein.